Contribution from the Department of Chemistry,
The University of Chicago, Chicago, Illinois 60637

Synthesis and Crystal and Molecular Structure of the Oxo-Bridged, Iron(III) Macrocyclic Dimer $[Fe(C_{22}H_{22}N_4)]_2O \cdot CH_3CN$: μ-Oxo-bis[7,16-dihydro-6,8,16,17-tetramethyldibenzo[*b*,*i*][1,4,8,11]tetraazacyclotetradecinato]-iron(III)–Acetonitrile

MARVIN C. WEISS and VIRGIL L. GOEDKEN*[1]

Received October 12, 1977

Oxygen reacts with the four-coordinate Fe(II) complex containing the dianionic, macrocyclic ligand $C_{22}H_{22}N_4^{2-}$ to yield the oxo-bridged dimer $[Fe(C_{22}H_{22}N_4)]_2O$. The crystal and molecular structure of the Fe(III) dimer has been determined from three-dimensional X-ray diffraction data. The crystal data are as follows: $[Fe(C_{22}H_{22}N_4)]_2O \cdot CH_3CN$, space group C_i^1-$P\bar{1}$ with $a = 11.941$ (2) Å, $b = 11.923$ (2) Å, $c = 17.051$ (3) Å, $\alpha = 78.21$ (1)°, $\beta = 71.09$ (1)°, and $\gamma = 66.58$ (1)° with $Z = 2$. The structure was refined by Fourier and least-squares techniques to conventional and weighted R values of 0.040 and 0.054, respectively, based on 8545 data with $|F_o| \geq 3\sigma(F_o)$. The macrocyclic ligand has the typical saddle shape exhibited in previously solved complexes containing the title macrocycle. The square-pyramidal coordination geometry and bond parameters indicate high-spin Fe(III): the average displacement of the Fe(III) from the N_4 donor plane is 0.698 Å, while the average Fe(III)–N distance is 2.054 Å. Departing significantly from linearity, the Fe(III)–O–Fe(III) angle is 142.78°. The room-temperature magnetic moment of the complex is 1.96 μ_B (per Fe) indicating antiferromagnetic coupling between the two Fe(III) centers. Infrared spectra show two Fe–O–Fe related vibrations at 890 and 882 cm^{-1}. These results are discussed along with comparisons drawn from the structures of the high-spin, five-coordinate Fe(III) complex $[Fe(C_{22}H_{22}N_4)Cl] \cdot CH_3CN$ and related mesotetraphenylporphyrin complexes.

Introduction

Considerable attention has been given to the structural characterization of five-coordinate Fe(III) complexes derived from macrocyclic or open-chain tetradentate ligands. A variety of Schiff-base tetradentate, macrocyclic, and porphyrin complexes of the type FeL–O–FeL[2-11] or FeLX[12-15] (X is halide or nitrogen base) have been structurally examined. Much interest has been generated for various reasons. Five-coordination in high-spin Fe(III) complexes has been established to be quite common as a result of the structural characterization of many square-pyramidal species derived from tetradentate, macrocyclic, and porphyrin ligands. The reaction mechanisms governing the formation of five-coordinate Fe(III) and μ-oxo-bridged Fe(III) species have excited interest because of their relevance to the functioning of metalloporphyrins in biological systems.[16,17] Also the property of antiferromagnetic spin coupling exhibited by complexes of the type FeL–O–FeL has received attention both because of the mechanistic importance of the coupling phenomena[18-21] and because of the fact that the oxo-bridged complexes may mimic function and model spin coupling in biologic systems.[22-27] Inherent in the crystal structure examinations is the elucidation of structural constraints which govern the solid-state electronic and magnetic properties of the complexes. Unfortunately, to date, no good structural–magnetic correlations have been established for the oxo-bridged systems, probably because the extent of bend in the Fe–O–Fe angle and concomitant π bonding through the oxygen bridge are poorly understood.[9,10,22]

The oxo-bridged dimer $[Fe(C_{22}H_{22}N_4)]_2O$, μ-oxo-bis-[7,16-dihydro-6,8,15,17-tetramethyldibenzo[*b*,*i*][1,4,8,11]-tetraazacyclotetradecinato]iron(III), was isolated initially as a byproduct of the reaction used to synthesize the high-spin five-coordinate complex $[Fe(C_{22}H_{22}N_4)Cl]$.[28] Since the structure of this complex had already been solved, the solution of the molecular structure of $[Fe(C_{22}H_{22}N_4)]_2O$ was undertaken for the following reasons: (1) to determine whether the change in μ_{eff} (5.95 μ_B for $[Fe(C_{22}H_{22}N_4)Cl]$ to 1.96 μ_B for $[Fe(C_{22}H_{22}N_4)]_2O$) or the close approach of two macrocyclic rings would change the structural parameters associated with the five-coordinate Fe(III) macrocyclic backbone; (2) to examine the close contacts between the macrocyclic species in each half of the dimer to determine the possible methods to use to couple the macrocyclic rings together in a rigid fashion, i.e., predict ideal chain length, functionality, etc., in a series of experiments designed to fix the macrocyclic into dimeric or oligomeric units; and (3) to make comparisons and elucidate contrasts between the $[Fe(C_{22}H_{22}N_4)Cl]$ and $[Fe(C_{22}H_{22}N_4)]_2O$ complexes and their mesotetraphenylporphyrin counterparts.

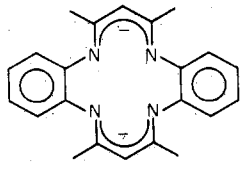

$C_{22}H_{22}N_4^{2-}$

Experimental Section

Synthesis of $[Fe(C_{22}H_{22}N_4)]_2O \cdot CH_3CN$. The free ligand $C_{22}H_{22}N_4$ was obtained as previously described.[29] The four-coordinate complex $[Fe(C_{22}H_{22}N_4)]$ was prepared by a modification of the reported procedures.[12] One equivalent of bis(*o*-phenylenediamine)bis(thiocyanato)iron(II), $[Fe(o\text{-}PDA)_2(NCS)_2]$, and 1 equiv of the free ligand were slurried in dry acetonitrile, under a nitrogen atmosphere, followed by the addition of 4 equiv of anhydrous triethylamine through a serum cap. After a few minutes the product crystallized from solution as dark red needles. The reaction vessel was then set aside for 24 h, during which time oxygen presumably leaks through the punctured serum cap. Attempts to hasten crystal growth of the product have been unsuccessful. The product slowly formed as uniform, intensely colored black crystals. The solution was filtered, washed with cold acetonitrile and diethyl ether, and dried in air. The compound is among the most oxygen-stable metal complexes of the $C_{22}H_{22}N_4^{2-}$ ligand prepared, the crystals showing no decomposition after one year. Anal. Calcd for $Fe_2C_{46}H_{47}N_9O$: C, 64.72; H, 5.5; N, 14.77. Found: C, 64.55; H, 5.43; N, 15.00.

Crystal Examination and Data Collection. Preliminary precession photographs of $[Fe(C_{22}H_{22}N_4)]_2O$ crystals showed that they belonged to the triclinic system requiring space group C_1^1-$P1$ or C_i^1-$P\bar{1}$.[30] The refined cell constants and other pertinent crystal data are listed in Table I.

0020-1669/79/1318-0819$01.00/0

Table I. Crystal Data for $[Fe(C_{22}H_{22}N_4)]_2O\cdot CH_3CN$

mol wt	853.64
space group	$P\bar{1}$
cell constants	
a, Å	11.941 (2)
b, Å	11.923 (2)
c, Å	17.051 (3)
α, deg	78.21 (1)
β β, deg	71.09 (1)
γ, deg	66.58 (1)
no. of reflections to cell constants	25
2θ limits, deg	$30 < 2\theta < 40$
Z	2
ρ_{calcd}, g/cm^3	1.35
ρ_{exptl}, g/cm^3	1.40
μ, cm^{-1}	7.59
absorption correction	none

Table II. Data Collection and Refinement Details for $[Fe(C_{22}H_{22}N_4)]_2O\cdot CH_3CN$[a]

diffractometer	Syntex $P2_1$
monochromator (Bragg angle, deg)	graphite (6.093)
radiation, Å	Mo Kα (0.710 69)
takeoff angle, deg	6.0
method	θ–2θ
scan speed, deg/min	variable scan speed depending on preliminary determination of peak intensity; speed varied from 2.0 to 29.3
scan width, deg	2.0
bkgd time/scan time	1.0
no. of standards	3
2θ limits of data, deg	$0 < 2\theta < 55$
no. of data collected	10 108
no. of data used in final refinement	8545, $\lvert F_o\rvert > 3\sigma(F_c)$
no. of data/no. of variables (NO/NV)	15.8
$R_1 = [\Sigma\lvert\lvert F_o\rvert - \lvert F_c\rvert\rvert/\Sigma\lvert F_o\rvert]$	0.040
$R_2 = [\Sigma w(\lvert F_o\rvert - \lvert F_c\rvert)^2/\Sigma w(F_o)^2]^{1/2}$	0.054
standard error in an observn of unit weight (=$[\Sigma w(\lvert F_o\rvert - \lvert F_c\rvert)^2/(NO - NV)]^{1/2}$), electrons	1.43
max residual electron density on final ΔF synthesis map, electrons Å^{-3}	0.329

[a] The function minimized was $\Sigma w(\lvert F_o\rvert - \lvert F_c\rvert)^2$, where $w = 1/\sigma(F_o)^2$.

Intensity data were collected on the Syntex $P2_1$ automated diffractometer by the θ–2θ scan technique; the routine aspects of data collection are presented in Table II. Examination of the crystal standards measured every 100 reflections revealed no crystal decomposition during the course of data collection.

Relative intensities of the data were calculated by $I = [S - (t_s/t_b)(B_1 + B_2)]R$, where S is the integrated peak intensity, B_1 and B_2 are the two background counts, R is the scan rate, and t_s/t_b is the ratio of total scan time to total background time. Observed structure factor amplitudes were calculated by using Azaroff's formula for the Lorentz and polarization factors (Lp) under the condition of monochromated radiation, $F_o = [I/(Lp)]^{1/2}$.[31] The standard deviations in I were estimated by $\sigma(I) = [\sigma_c(I)^2 + (pI)^2]^{1/2}R$, where $\sigma_c(I)$ is the standard deviation from counting statistics, $\sigma_c(I) = [S + (t_s/t_b)^2(B_1 + B_2)]^{1/2}$, and p is a factor, taken here to be 0.02, to account for machine fluctuations and other sources of error which would be expected to result in variations proportional to the diffracted intensity.[32,33] Standard deviations in $\lvert F_o\rvert$ were calculated as $\sigma(F_o) = \sigma(F_o^2)/2F_o$, where $\sigma(F_o^2) = \sigma(I)/(Lp)$.

Solution and Refinement. Normalized structure factor amplitudes were calculated via Wilson's method, and the E statistics indicated a centric structure.[34,35] The two Fe atoms were located from a Patterson map. Subsequent Fourier maps based upon the heavy-atom phases and observed structure factor amplitudes revealed the positions of the nonhydrogen atoms in the macrocyclic framework and the oxygen bridge. After refinement of the positional and isotropic thermal parameters for the nonhydrogen atoms, a difference Fourier map revealed a disordered acetonitrile solvate molecule. The solvate molecule was fitted by assuming 0.5 occupancy for each of two linear units pivoted on the methyl carbon atom of the acetonitrile, the units forming an angle of approximately 70°. Full-matrix least-squares refinement of positional and isotropic thermal parameters for all nonhydrogen atoms and occupancies for the two solvent units reduced the conventional and weighted R values to 0.102 and 0.135, respectively. A difference Fourier map then revealed the position of all hydrogen atoms associated with the macrocyclic unit. Using as trial coordinates the peaks associated with the methyl carbons, we calculated hydrogen atom positions with the assumption of standard tetrahedral geometry and C–H distances of 0.98 Å.[36] The coordinates for all other macrocyclic hydrogen atoms were calculated (C–H = 0.98 Å) while two sets of methyl hydrogens were fixed at random orientations corresponding to two disordered solvent units, each set with an occupancy of 0.5. Included as fixed contributions in the final refinement, all hydrogen atoms were assigned isotropic temperature factors equal to 5.0 Å^2.

Because of the large number of variables (541), the final refinement proceeded utilizing block-matrix least-squares techniques with variation of positional and anisotropic thermal parameters for all nonhydrogen atoms. Occupancies for the solvate molecule were fixed at 1.0 for the pivot methyl carbon and 0.5 for atoms in the two acetonitrile units. After each block had been refined twice, the model converged at conventional and weighted R values of 0.040 and 0.054, respectively. Refinement details and final agreement indices are listed in Table II. The final difference Fourier map was featureless, with the maximum residual electron density of 0.329 Å^{-3} near one of the solvate acetonitrile units. The final positional and thermal parameters, along with their estimated standard deviations are listed in Tables III and IV. Observed and calculated structure factor amplitudes and hydrogen atom coordinates are available.[37]

Results and Discussion of the Structure

Synthesis. The four-coordinate $[Fe(C_{22}H_{22}N_4)]$ species and a variety of its carbon monoxide adducts have been structurally characterized[38,39] As previously described,[12,40] whenever attempts are made to synthesize the four-coordinate $[Fe(C_{22}H_{22}N_4)]$ species in the presence of perchlorate, the major product is always the five-coordinate species $[Fe(C_{22}H_{22}N_4)Cl]$, presumably because of a redox reaction between the Fe(II) species and the ClO_4^- anion to give Fe(III) and Cl^-. However, when the insertion reaction is carried out in the absence of perchlorate or any other oxidizing species, $[Fe(C_{22}H_{22}N_4)]$ is formed. When any of the Fe(II) species, isolated or generated in situ, is exposed to a small amount of oxygen, the complex readily decomposes to give the oxo-bridged species $[Fe(C_{22}N_{22}H_4)]_2O$. The isolated complex is remarkably insoluble and is one of the most robust of all the five-coordinate species derived from this macrocyclic ligand.

General Description of the Structure. The structure of the oxo-bridged Fe(III) species reveals two five-coordinate macrocyclic units, joined by a bridging oxygen atom, with a Fe–O–Fe angle of 142.75°. The Fe(III) atoms are displaced from the mean plane formed from the four nitrogen donor atoms (Fe–N_4 distance) by an average distance of 0.698 Å. The asymmetric unit contains one molecule of acetonitrile trapped in a rather large lattice cavity formed by the loose packing of the dimeric units. The closest contact of the solvate molecule with the complex is 3.395 Å (O–C1A); the lack of any close contact coupled with the large lattice cavity has allowed the acetonitrile solvate to disorder in an unusual V shape. The solvate is distributed over two sites, each with approximately 50% occupancy, and pivoted on the methyl carbon forming an angle of 75.8°.

The macrocyclic ligand in both halves of the dimer has the usual saddle shape previously reported. Views of the complex normal to the plane described by the Fe–O–Fe atoms and parallel to the Fe–Fe axis are presented in Figures 1 and 2. The packing of the complex and solvent molecule in the unit

Table III. Nonhydrogen Atom Positional Parameters for $[Fe(C_{22}H_{22}N_4)]_2O\cdot CH_3CN$

atom	*x*	*y*	*z*
Fe-1	0.02575 (3)	0.19019 (3)	0.12656 (2)
N1-1	−0.1004 (2)	0.1250 (2)	0.1125 (1)
N2-1	0.1433 (2)	0.0113 (2)	0.1430 (1)
N3-1	0.2016 (2)	0.2002 (2)	0.0683 (1)
N4-1	−0.0411 (2)	0.3128 (2)	0.0331 (1)
C1-1	−0.0848 (2)	0.0097 (2)	0.1058 (1)
C2-1	0.0251 (2)	−0.0897 (2)	0.1137 (1)
C3-1	0.1343 (2)	−0.0898 (2)	0.1281 (1)
C4-1	0.2518 (2)	0.0157 (2)	0.1570 (1)
C5-1	0.3180 (2)	−0.0643 (2)	0.2124 (1)
C6-1	0.4167 (2)	−0.0440 (3)	0.2260 (2)
C7-1	0.4475 (2)	0.0561 (3)	0.1860 (2)
C8-1	0.3813 (2)	0.1393 (3)	0.1324 (2)
C9-1	0.2834 (2)	0.1192 (2)	0.1159 (1)
C10-1	0.2398 (2)	0.2515 (2)	−0.0075 (1)
C11-1	0.1557 (3)	0.3288 (2)	−0.0533 (1)
C12-1	0.0242 (2)	0.3582 (2)	−0.0363 (1)
C13-1	−0.1717 (2)	0.3316 (2)	0.0532 (1)
C14-1	−0.2692 (3)	0.4413 (2)	0.0397 (2)
C15-1	−0.3949 (3)	0.4502 (2)	0.0693 (2)
C16-1	−0.4259 (2)	0.3512 (3)	0.1160 (2)
C17-1	−0.3314 (2)	0.2430 (2)	0.1318 (2)
C18-1	−0.2039 (2)	0.2293 (2)	0.0983 (1)
C19-1	−0.1821 (2)	−0.0206 (2)	0.0840 (2)
C20-1	0.2464 (2)	−0.2100 (2)	0.1194 (2)
C21-1	0.3800 (3)	0.2217 (3)	−0.0510 (2)
C22-1	−0.0352 (3)	0.4368 (3)	−0.1045 (2)
O	−0.0411 (1)	0.2621 (1)	0.2222 (1)
Fe-2	−0.05681 (3)	0.23140 (3)	0.33174 (2)
N1-2	0.1081 (2)	0.2103 (2)	0.3555 (1)
N2-2	−0.0207 (2)	0.0482 (2)	0.3638 (1)
N3-2	−0.2355 (2)	0.2290 (2)	0.3947 (1)
N4-2	−0.1062 (2)	0.3918 (2)	0.3840 (1)
C1-2	0.1802 (2)	0.1128 (2)	0.3937 (1)
C2-2	0.1635 (2)	0.0004 (2)	0.4102 (1)
C3-2	0.0708 (2)	−0.0325 (2)	0.3970 (1)
C4-2	−0.1224 (2)	0.0245 (2)	0.3552 (1)
C5-2	−0.1141 (2)	−0.0789 (2)	0.3247 (1)
C6-2	−0.2217 (3)	−0.0890 (3)	0.3157 (2)
C7-2	−0.3362 (3)	0.0062 (3)	0.3349 (2)
C8-2	−0.3459 (2)	0.1124 (3)	0.3610 (2)
C9-2	−0.2411 (2)	0.1231 (2)	0.3734 (1)
C10-2	−0.3228 (2)	0.2995 (2)	0.4546 (1)
C11-2	−0.3098 (2)	0.4005 (2)	0.4753 (1)
C12-2	−0.2071 (2)	0.4415 (2)	0.4454 (1)
C13-2	0.0009 (2)	0.4265 (2)	0.3543 (1)
C14-2	−0.0006 (3)	0.5466 (2)	0.3315 (2)
C15-2	0.1113 (3)	0.5678 (2)	0.2959 (2)
C16-2	0.2261 (3)	0.4715 (3)	0.2803 (2)
C17-2	0.2293 (3)	0.3517 (2)	0.2998 (2)
C18-2	0.1183 (2)	0.3277 (2)	0.3381 (1)
C19-2	0.2800 (3)	0.1216 (3)	0.4264 (2)
C20-2	0.0774 (2)	−0.1632 (2)	0.4259 (1)
C21-2	−0.4379 (2)	0.2699 (3)	0.5073 (2)
C22-2	−0.2129 (3)	0.5412 (3)	0.4912 (2)
C1-A	−0.3329 (4)	−0.5140 (3)	0.2575 (2)
C2-A	−0.4610 (7)	−0.4380 (6)	0.2730 (4)
C2-A′	−0.3359 (7)	−0.4016 (7)	0.2777 (4)
N-A	−0.5636 (8)	−0.3755 (8)	0.2888 (6)
N-A′	−0.3314 (8)	−0.3141 (7)	0.2924 (5)

cell is shown in two perspectives in Figures 3 and 4. Bond distances and angles are listed in Tables V and VI (refer to Figure 5 for a description of the labeling scheme employed for the macrocyclic backbone), and selected dihedral angles are listed in Tables VII and VIII. .

Examination of the structure reveals that the bond distances and angles in the macrocyclic ligand are essentially identical with chemically equivalent distances and angles in other complexes of the ligand structurally characterized. Bonding patterns describing a 16π-electron ring system which is not delocalized are maintained; i.e., the delocalized 2,4-pentanediiminato chelate rings are separated from the aromatic benzenoid rings by nominally single C–N bonds (the average

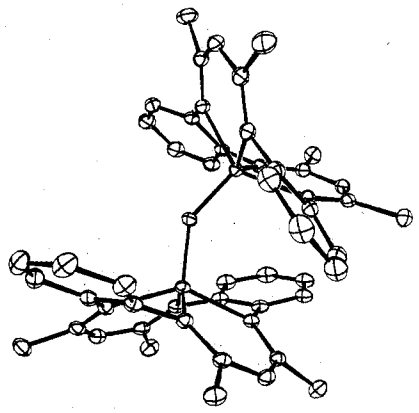

Figure 1. Side view of the dimeric unit $[Fe(C_{22}H_{22}N_4)]_2O$ viewed normal to the plane formed by atoms Fe–O–Fe. The thermal ellipsoids are drawn at the 20% probability level.

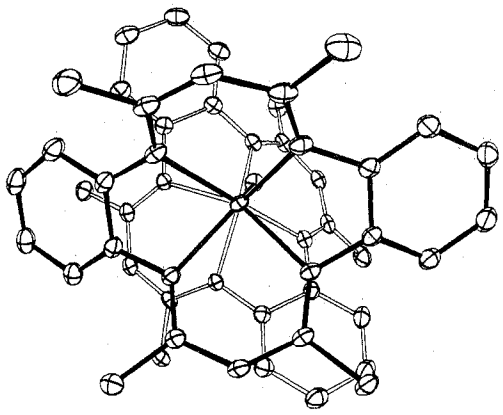

Figure 2. View of the dimeric unit $[Fe(C_{22}H_{22}N_4)]_2O$ as viewed down the Fe–Fe bond axis. The thermal ellipsoids are drawn at the 20% probability level.

C–N bond is 1.412 Å). The average maximum deviation from the 2,4-pentanediiminato chelate ring is 0.09 Å for the Fe atom (0.01 Å for the others). The benzenoid ring is rigorously planar: the maximum deviation from the six-atom plane is 0.015 Å. Other points of structural interest involving the Fe(III) macrocyclic backbone will be discussed later.

Parameters characterizing the Fe–O–Fe bridge are of considerable interest. The average Fe–O bond distance, 1.792 Å, is in the range of 1.76–1.80 Å spanned by related structures. The Fe–O–Fe angle, 142.75°, is closer to that observed in the flexible salen derivatives (139–145°)[5,6] than that in $[Fe(TPP)]_2O$ (174.5°).[5] Table IX lists the important averaged structural parameters for a variety of oxo-bridged species. Explanations of the wide range of Fe–O–Fe angles have involved analysis of the conformation and flexibility of the equatorial ligands. The extent to which this angle is dependent upon electronic factors, steric interactions of the large planar ligands, and packing arrangements in the lattice are difficult to evaluate. The oxo-bridged complexes of the more rigid and bulky ligands (TPP[2,3] and the rigid salen[4,5] derivatives) encounter increasingly greater steric repulsions as the M–O–M angle decreases. The extent of Fe $d\pi$ and O $p\pi$ orbital interaction should be enhanced by a linear configuration of the three atoms. The Fe–O distance of the TPP complex is shorter than the analogous distances of the salen or $C_{22}H_{22}N_4^{2-}$ complexes, consistent with this interpretation, but any substantial deviation from a nonlinear Fe–O–Fe bond of the porphyrin complex is prohibited by the extensive peripheral framework of the ms-TPP ligand. The cone-shaped flexible salen oxo-bridged dimers exhibit close contacts between opposing benzene residuals (approximately 3.40 Å). These

Table IV. Nonhydrogen Atom Anisotropic Thermal Parameters for $[Fe(C_{22}H_{22}N_4)]_2O\cdot CH_3CN$[a]

atom	β_{11}	β_{22}	β_{33}	β_{12}	β_{13}	β_{23}
Fe-1	0.00672 (3)	0.00606 (2)	0.00251 (1)	−0.00322 (2)	−0.00108 (1)	−0.00081 (1)
N1-1	0.0074 (2)	0.0061 (1)	0.0031 (1)	−0.0031 (1)	−0.0014 (1)	−0.0007 (1)
N2-1	0.0063 (2)	0.0067 (1)	0.0030 (1)	−0.0030 (1)	−0.0010 (1)	−0.0009 (1)
N3-1	0.0081 (2)	0.0080 (2)	0.0032 (1)	−0.0047 (1)	−0.0005 (1)	−0.0012 (1)
N4-1	0.0096 (2)	0.0067 (1)	0.0029 (1)	−0.0043 (1)	−0.0018 (1)	−0.0005 (1)
C1-1	0.0075 (2)	0.0072 (2)	0.0028 (1)	−0.0041 (1)	−0.0008 (1)	−0.0010 (1)
C2-1	0.0084 (2)	0.0064 (2)	0.0035 (1)	−0.0040 (2)	−0.0012 (1)	−0.0008 (1)
C3-1	0.0073 (2)	0.0068 (2)	0.0029 (1)	−0.0032 (2)	−0.0009 (1)	−0.0007 (1)
C4-1	0.0061 (2)	0.0080 (2)	0.0033 (1)	−0.0026 (2)	−0.0008 (1)	−0.0019 (1)
C5-1	0.0072 (2)	0.0094 (2)	0.0036 (2)	−0.0021 (2)	−0.0013 (1)	−0.0018 (1)
C6-1	0.0076 (2)	0.0122 (3)	0.0045 (1)	−0.0018 (2)	−0.0021 (1)	−0.0026 (1)
C7-1	0.0073 (2)	0.0146 (3)	0.0062 (1)	−0.0040 (2)	−0.0020 (1)	−0.0034 (2)
C8-1	0.0087 (2)	0.0117 (3)	0.0053 (1)	−0.0057 (2)	−0.0011 (1)	−0.0023 (1)
C9-1	0.0063 (2)	0.0087 (2)	0.0036 (1)	−0.0035 (2)	−0.0005 (1)	−0.0019 (1)
C10-1	0.0103 (2)	0.0074 (2)	0.0035 (1)	−0.0054 (2)	0.0001 (1)	−0.0014 (1)
C11-1	0.0127 (3)	0.0080 (2)	0.0030 (1)	−0.0064 (2)	−0.0001 (1)	−0.0006 (1)
C12-1	0.0133 (3)	0.0069 (2)	0.0029 (1)	−0.0054 (2)	−0.0019 (1)	−0.0006 (1)
C13-1	0.0094 (2)	0.0070 (2)	0.0033 (1)	−0.0036 (2)	−0.0025 (1)	−0.0008 (1)
C14-1	0.0125 (3)	0.0071 (2)	0.0051 (1)	−0.0035 (2)	−0.0043 (2)	−0.0006 (1)
C15-1	0.0111 (3)	0.0083 (2)	0.0075 (2)	−0.0015 (2)	−0.0056 (2)	−0.0016 (2)
C16-1	0.0082 (2)	0.0100 (3)	0.0075 (2)	−0.0025 (2)	−0.0033 (2)	−0.0026 (2)
C17-1	0.0082 (2)	0.0085 (2)	0.0053 (1)	−0.0036 (2)	−0.0019 (1)	−0.0015 (1)
C18-1	0.0083 (2)	0.0070 (2)	0.0035 (1)	−0.0033 (2)	−0.0023 (1)	−0.0010 (1)
C19-1	0.0087 (2)	0.0086 (2)	0.0044 (1)	−0.0049 (2)	−0.0016 (1)	−0.0015 (1)
C20-1	0.0097 (3)	0.0068 (2)	0.0055 (1)	−0.0023 (2)	−0.0023 (1)	−0.0014 (1)
C21-1	0.0112 (3)	0.0105 (3)	0.0051 (1)	−0.0049 (2)	0.0015 (2)	−0.0013 (1)
C22-1	0.0183 (4)	0.0106 (3)	0.0034 (1)	−0.0068 (3)	−0.0034 (2)	0.0008 (1)
O	0.0071 (1)	0.0072 (1)	0.0024 (1)	−0.0026 (1)	−0.0013 (1)	−0.0009 (1)
Fe-2	0.00673 (3)	0.00592 (2)	0.00251 (1)	−0.00132 (2)	−0.00144 (1)	−0.00067 (1)
N1-2	0.0072 (2)	0.0069 (2)	0.0032 (1)	−0.0019 (1)	−0.0016 (1)	−0.0008 (1)
N2-2	0.0067 (2)	0.0065 (1)	0.0029 (1)	−0.0016 (1)	−0.0015 (1)	−0.0003 (1)
N3-2	0.0069 (2)	0.0072 (1)	0.0033 (1)	−0.0010 (1)	−0.0016 (1)	−0.0004 (1)
N4-2	0.0085 (2)	0.0066 (2)	0.0030 (1)	−0.0010 (1)	−0.0018 (1)	−0.0012 (1)
C1-2	0.0068 (2)	0.0080 (2)	0.0031 (1)	−0.0014 (2)	−0.0015 (2)	−0.0011 (1)
C2-2	0.0070 (2)	0.0073 (2)	0.0032 (1)	−0.0009 (2)	−0.0019 (1)	−0.0005 (1)
C3-2	0.0071 (2)	0.0063 (2)	0.0025 (2)	−0.0007 (1)	−0.0010 (1)	−0.0006 (1)
C4-2	0.0080 (2)	0.0073 (2)	0.0029 (1)	−0.0026 (2)	−0.0017 (1)	0.0001 (1)
C5-2	0.0105 (3)	0.0082 (2)	0.0038 (1)	−0.0035 (2)	−0.0025 (1)	−0.0003 (1)
C6-2	0.0140 (3)	0.0109 (3)	0.0049 (1)	−0.0064 (3)	−0.0039 (2)	0.0000 (1)
C7-2	0.0119 (3)	0.0136 (3)	0.0058 (1)	−0.0068 (3)	−0.0042 (2)	0.0005 (2)
C8-2	0.0083 (2)	0.0120 (3)	0.0052 (1)	−0.0034 (2)	−0.0029 (1)	0.0000 (1)
C9-2	0.0076 (2)	0.0082 (2)	0.0033 (1)	−0.0024 (2)	−0.0017 (1)	0.0001 (1)
C10-2	0.0066 (2)	0.0083 (2)	0.0037 (1)	−0.0001 (2)	−0.0015 (1)	−0.0003 (1)
C11-2	0.0079 (2)	0.0083 (2)	0.0034 (1)	0.0006 (2)	−0.0014 (1)	−0.0011 (1)
C12-2	0.0092 (2)	0.0073 (2)	0.0033 (1)	0.0002 (2)	−0.0025 (1)	−0.0012 (1)
C13-2	0.0099 (2)	0.0071 (2)	0.0030 (1)	−0.0025 (2)	−0.0019 (1)	−0.0012 (1)
C14-2	0.0138 (3)	0.0074 (2)	0.0042 (1)	−0.0031 (2)	−0.0025 (1)	−0.0011 (1)
C15-2	0.0171 (4)	0.0088 (2)	0.0049 (1)	−0.0062 (3)	−0.0018 (2)	−0.0012 (1)
C16-2	0.0146 (3)	0.0116 (3)	0.0048 (1)	−0.0078 (3)	−0.0011 (2)	−0.0013 (1)
C17-2	0.0108 (3)	0.0100 (2)	0.0042 (1)	−0.0046 (2)	−0.0013 (1)	−0.0016 (1)
C18-2	0.0093 (2)	0.0078 (2)	0.0030 (1)	−0.0032 (2)	−0.0017 (1)	−0.0009 (1)
C19-2	0.0097 (3)	0.0116 (3)	0.0054 (1)	−0.0037 (2)	−0.0038 (2)	−0.0005 (1)
C20-2	0.0101 (2)	0.0064 (2)	0.0039 (1)	−0.0016 (2)	−0.0024 (1)	0.0000 (1)
C21-2	0.0078 (2)	0.0117 (3)	0.0057 (1)	−0.0010 (2)	0.0000 (1)	−0.0010 (2)
C22-2	0.0118 (3)	0.0117 (3)	0.0048 (1)	−0.0011 (2)	−0.0016 (2)	−0.0040 (1)
C1-A	0.0193 (5)	0.0147 (4)	0.0059 (2)	−0.0031 (4)	−0.0056 (2)	0.0004 (2)
C2-A	0.0149 (8)	0.0123 (7)	0.0054 (3)	−0.0039 (6)	−0.0030 (4)	−0.0006 (3)
C2-A′	0.0138 (8)	0.0140 (8)	0.0046 (3)	−0.0014 (6)	−0.0022 (4)	−0.0005 (4)
N-A	0.0205 (11)	0.0196 (10)	0.0122 (6)	−0.0023 (9)	−0.0056 (7)	−0.0040 (6)
N-A′	0.0256 (12)	0.0179 (9)	0.0082 (4)	−0.0073 (9)	−0.0045 (6)	−0.0016 (5)

[a] Anisotropic thermal parameters are of the form $\exp[-(h^2\beta_{11} + k^2\beta_{22} + l^2\beta_{33} + 2hk\beta_{12} + 2hl\beta_{13} + 2kl\beta_{23})]$.

considerations are applicable to the present case; the pronounced saddle conformation of the macrocycle allows a more intimate (but noninteractive) packing than that allowed by the mesotetraphenylporphyrin ligand. As can be seen in Figures 1 and 2 and in the stereodiagrams in Figures 3 and 4, the two halves of the dimer fit snugly together. The Fe–O–Fe angle departs from linearity such that a 2,4-pentanediiminato chelate ring and a benzenoid ring of one macrocycle approximately stack over a benzenoid ring and a 2,4-pentanediiminato chelate ring, respectively, of the other macrocyclic ring. The closest contacts between halves of the dimer are made in this interaction and are 3.445 Å (C2-1, C5-2) and 3.359 Å (C5-1, C2-2). It is obvious from this result, that considerable thought and effort be directed to covalently linking the two halves.

Comparisons of $[Fe(C_{22}H_{22}N)]_2O$ with $[Fe(C_{22}H_{22}N_4)Cl]$ and Parallels with the Related Mesotetraphenylporphyrin Structures. Since both derivatives of the ligand are five-coordinate square-pyramidal Fe(III) complexes, numerous structural features are related and a discussion of similarities and slight differences is useful. Listed in Table X are a variety of average structural parameters for $[Fe(C_{22}H_{22}N_4)]_2O$ and $[Fe(C_{22}H_{22}N_4)Cl]$ which have proven useful in describing the structural features and tendencies of the title macrocycle and

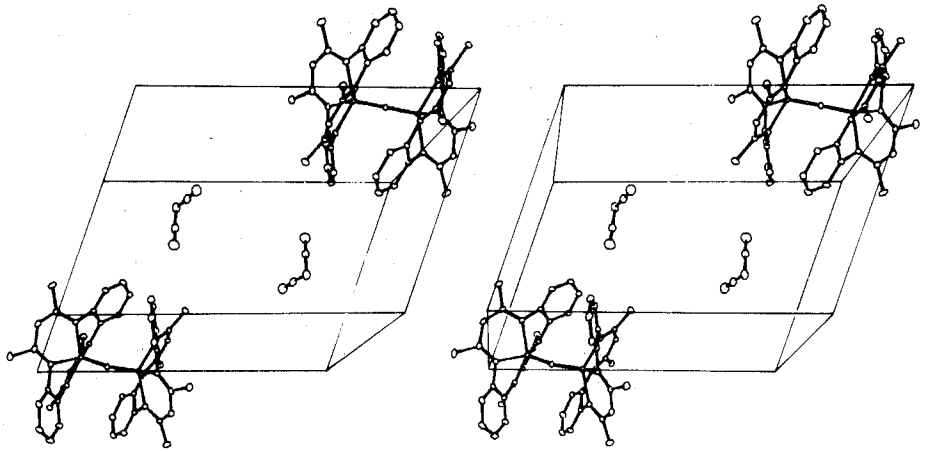

Figure 3. Stereoscopic diagram of the unit cell contents and packing arrangement of $[Fe(C_{22}H_{22}N_4)]_2O\cdot CH_3CN$ as viewed down the axis normal to the *bc* crystallographic face. The acetonitrile solvent molecule is shown in its disordered configuration. The thermal ellipsoids are drawn at the 10% probability level.

Table V. Selected Bond Distances (Å) for $[Fe(C_{22}H_{22}N_4)]_2O\cdot CH_3CN$

Fe-1	O	1.793 (1)	Fe-2	O	1.791 (1)
Fe-1	N1-1	2.042 (2)	Fe-2	N1-2	2.046 (2)
Fe-1	N2-1	2.052 (2)	Fe-2	N2-2	2.042 (2)
Fe-1	N3-1	2.056 (2)	Fe-2	N3-2	2.063 (2)
Fe-1	N4-1	2.063 (2)	Fe-2	N4-2	2.064 (2)
N1-1	C1-1	1.336 (2)	N1-2	C1-2	1.333 (3)
N1-1	C18-1	1.408 (3)	N1-2	C18-2	1.416 (3)
N2-1	C3-1	1.332 (3)	N2-2	C3-2	1.334 (3)
N2-1	C4-1	1.413 (3)	N2-2	C4-2	1.408 (3)
N3-1	C9-1	1.409 (3)	N3-2	C9-2	1.415 (3)
N3-1	C10-1	1.331 (3)	N3-2	C10-2	1.342 (3)
N4-1	C12-1	1.334 (3)	N4-2	C12-2	1.330 (3)
N4-1	C13-1	1.417 (3)	N4-2	C13-2	1.407 (3)
C1-1	C2-1	1.399 (3)	C1-2	C2-2	1.393 (3)
C1-1	C19-1	1.513 (3)	C1-2	C19-2	1.514 (3)
C2-1	C3-1	1.403 (3)	C2-2	C3-2	1.405 (3)
C3-1	C20-1	1.516 (3)	C3-2	C20-2	1.513 (3)
C4-1	C5-1	1.393 (3)	C4-2	C5-2	1.390 (3)
C4-1	C9-1	1.415 (3)	C4-2	C9-2	1.423 (3)
C5-1	C6-1	1.389 (3)	C5-2	C6-2	1.396 (4)
C6-1	C7-1	1.371 (4)	C6-2	C7-2	1.376 (4)
C7-1	C8-1	1.385 (4)	C7-2	C8-2	1.376 (4)
C8-1	C9-1	1.404 (3)	C8-2	C9-2	1.391 (3)
C10-1	C11-1	1.396 (4)	C10-2	C11-2	1.399 (4)
C10-1	C21-1	1.520 (4)	C10-2	C21-2	1.509 (4)
C11-1	C12-1	1.407 (4)	C11-2	C12-2	1.405 (4)
C12-1	C22-1	1.516 (3)	C12-2	C22-2	1.518 (3)
C13-1	C14-1	1.400 (3)	C13-2	C14-2	1.399 (3)
C13-1	C18-1	1.422 (13)	C13-2	C18-2	1.413 (3)
C14-1	C15-1	1.387 (4)	C14-2	C15-2	1.378 (4)
C15-1	C16-1	1.392 (4)	C15-2	C16-2	1.380 (4)
C16-1	C17-1	1.381 (4)	C16-2	C17-2	1.387 (4)
C17-1	C18-1	1.395 (3)	C17-2	C18-2	1.389 (3)
C1-A	C2-A	1.402 (8)			
C1-A	C2-A′	1.434 (9)			
C2-A	N1-A	1.129 (9)			
C2-A′	N1-A′	1.146 (10)			

its metal derivatives. Along with the parameters particular to the macrocycle under study are some salient comparisons drawn from the structural determinations of the related tetraphenylporphyrin complexes $[Fe(TPP)]_2O$[3] and [Fe(TPP)Cl].[40]

An examination of parameters listed in Table X reveals that the complex $[Fe(C_{22}H_{22}N_4)]_2O$ exhibits a slight exaggeration of the coordination geometry of the high-spin square-pyramidal counterpart $[Fe(C_{22}H_{22}N_4)Cl]$. For example, there is a slight increase in the sum of the ten interior and four exterior angles of 5.0° (refer to Figure 6). Since the chemically equivalent bond distances are essentially identical, this macrocycle expansion alone allows for the increase of the N–Ct distance from 1.910 Å for the monomeric high-spin species to 1.931 Å for the oxo-bridged dimer. Another feature which parallels this trend is the degree of torsional twist about the C–N bonds in the five- and six-membered chelate rings (Table X). Indeed, the ring expansion and the torsional angle distribution indicate a larger radius for Fe(III) for the oxo-bridged species; consequently, the macrocycle has deformed to accomodate the modest increase in metal ion radius indicated by increased Fe–N (2.002 Å for the monomer to 2.054 Å for the dimer) and $Fe–N_4$ (0.600 to 0.698 Å) distances, where $Fe–N_4$ is the displacement of Fe from the N_4 donor plane. Alternative explanations for the increase in the Fe–N and $Fe–N_4$ distances in going from the high-spin $[Fe(C_{22}H_{22}N_4)Cl]$ to the oxo-bridged $[Fe(C_{22}H_{22}N_4)]_2O$ appear to be of limited importance. The very strong Fe–O bond could lead to a weakening and therefore lengthening of the Fe–N distances; however, it is unlikely that this would also produce an increase in the $Fe–N_4$ distance. Although steric interactions could conceivably lead to similar types of changes in bond parameters, there appears to be no need to invoke such remote possibilities in the light of more supportive evidence.

The magnetic moment 1.96 μ_B is consistent with either antiferromagnetically coupled high-spin iron(III) or a low-spin Fe(II) species. However, the Fe–N distance of 2.054 Å for the dimer is markedly longer than that for the low-spin Fe(II)–alkyl complex $[Fe(C_{22}N_{22}H_4)CH_3]$,[44] 1.908 Å, and conclusively supports the high-spin Fe(III) formulation.

Simple bonding arguments predict charge donation from the oxo ligand to Fe(III) via the Fe $d\pi$–O $p\pi$ interaction and normal σ bonding. Some radial expansion and increase in the Fe–N and $Fe–N_4$ distances are expected. The same trend is observed in analogous porphyrin complexes (Table X) and also in Cr(III) complexes. While the Fe–N distances of the porphyrin complexes are still shorter than observed in nonmacrocyclic systems, they are increased over their tetramethyldibenzotetraaza[14]annulene counterparts. Interestingly, there is a slight increase in the Fe–N and $Fe–N_4$ distances with a concomitant increase in the N–Ct distance on going from [Fe(TPP)Cl] to $[Fe(TPP)]_2O$. The magnitude of increase in bond parameters is almost identical with that observed in the complexes derived from the $C_{22}H_{22}N_4^{2-}$ ligand. The closest approach of the porphyrin planes in the oxo-bridged dimer of 5.20 Å is sufficient to eliminate nonbonding steric interactions as a source of displacement of Fe from the N_4 plane. Increases in metal–nitrogen distances, from 2.064 to 2.115 Å, on going from $[Cr(NH_3)_6]^{3+}$ to the oxo-bridged $[Cr(NH_3)_5]O^{4+}$ cation,[41,42] are in total accord with the previous conclusions.

Table VI. Selected Bond Angles (deg) for $[Fe(C_{22}H_{22}N_4)]_2O\cdot CH_3CN$

O	Fe-1	N1-1	108.40 (7)	O	Fe-2	N1-2	110.00 (5)
O	Fe-1	N2-1	111.17 (7)	O	Fe-2	N2-2	109.09 (5)
O	Fe-1	N3-1	110.40 (7)	O	Fe-2	N3-2	110.29 (5)
O	Fe-1	N4-1	109.65 (6)	O	Fe-2	N4-2	110.07 (5)
N1-1	Fe-1	N2-1	88.17 (7)	N1-2	Fe-2	N2-2	89.10 (7)
N1-1	Fe-1	N4-1	78.50 (7)	N1-2	Fe-2	N4-2	78.00 (7)
N2-1	Fe-1	N3-1	77.96 (7)	N2-2	Fe-2	N3-2	78.13 (7)
N3-1	Fe-1	N4-1	88.66 (7)	N3-2	Fe-2	N4-2	88.14 (7)
N1-1	Fe-1	N3-1	141.20 (7)	N1-2	Fe-2	N3-2	139.71 (7)
N2-1	Fe-1	N4-1	139.18 (7)	N2-2	Fe-2	N4-2	140.84 (7)
Fe-1	N1-1	C1-1	128.8 (1)	Fe-2	N1-2	C1-2	127.4 (2)
Fe-1	N1-1	C18-1	105.8 (1)	Fe-2	N1-2	C18-2	106.2 (1)
C1-1	N1-1	C18-1	124.8 (2)	C1-2	N1-2	C18-2	125.3 (2)
Fe-1	N2-1	C3-1	128.0 (2)	Fe-2	N2-2	C3-2	128.1 (1)
Fe-1	N2-1	C4-1	106.6 (1)	Fe-2	N2-2	C4-2	106.5 (1)
C3-1	N2-1	C4-1	124.3 (2)	C3-2	N2-2	C4-2	124.9 (2)
Fe-1	N3-1	C9-1	106.5 (1)	Fe-2	N3-2	C9-2	106.2 (1)
Fe-1	N3-1	C10-1	127.6 (2)	Fe-2	N3-2	C10-2	128.1 (2)
C9-1	N3-1	C10-1	124.6 (2)	C9-2	N3-2	C10-2	124.9 (2)
Fe-1	N4-1	C12-1	128.4 (2)	Fe-2	N4-2	C12-2	128.1 (2)
Fe-1	N4-1	C13-1	105.8 (1)	Fe-2	N4-2	C13-2	106.1 (1)
C12-1	N4-1	C13-1	125.5 (2)	C12-2	N4-2	C13-2	124.7 (2)
N1-1	C1-1	C2-1	122.4 (2)	N1-2	C1-2	C2-2	122.4 (2)
N1-1	C1-1	C19-1	121.8 (2)	N1-2	C1-2	C19-2	121.1 (2)
C2-1	C1-1	C19-1	115.6 (2)	C2-2	C1-2	C19-2	116.4 (2)
C1-1	C2-1	C3-1	128.9 (2)	C1-2	C2-2	C3-2	130.0 (2)
N2-1	C3-1	C2-1	122.4 (2)	N2-2	C3-2	C2-2	121.9 (2)
N2-1	C3-1	C20-1	121.2 (2)	N2-2	C3-2	C20-2	122.0 (2)
C2-1	C3-1	C20-1	116.2 (2)	C2-2	C3-2	C20-2	116.1 (2)
N2-1	C4-1	C5-1	125.6 (2)	N2-2	C4-2	C5-2	126.2 (2)
N2-1	C4-1	C9-1	114.1 (2)	N2-2	C4-2	C9-2	114.4 (2)
C5-1	C4-1	C9-1	120.0 (2)	C5-2	C4-2	C9-2	119.1 (2)
C4-1	C5-1	C6-1	120.1 (2)	C4-2	C5-2	C6-2	120.7 (2)
C5-1	C6-1	C7-1	119.9 (3)	C5-2	C6-2	C7-2	119.4 (2)
C6-1	C7-1	C8-1	121.5 (2)	C6-2	C7-2	C8-2	121.1 (2)
C7-1	C8-1	C9-1	119.7 (2)	C7-2	C8-2	C9-2	120.6 (2)
N3-1	C9-1	C4-1	114.9 (2)	N3-2	C9-2	C4-2	114.3 (2)
N3-1	C9-1	C8-1	126.0 (2)	N3-2	C9-2	C8-2	126.4 (2)
C4-1	C9-1	C8-1	118.7 (2)	C4-2	C9-2	C8-2	119.0 (2)
N3-1	C10-1	C11-1	122.7 (2)	N3-2	C10-2	C11-2	122.4 (2)
N3-1	C10-1	C21-1	120.9 (2)	N3-2	C10-2	C21-2	121.7 (2)
C11-1	C10-1	C21-1	116.3 (2)	C11-2	C10-2	C22-2	115.8 (2)
C10-1	C11-1	C12-1	129.8 (2)	C10-2	C11-2	C12-2	129.2 (2)
N4-1	C12-1	C11-1	121.7 (2)	N4-2	C12-2	C11-2	122.7 (2)
N4-1	C12-1	C22-1	122.7 (2)	N4-2	C12-2	C22-2	121.0 (2)
C11-1	C12-1	C22-2	115.5 (2)	C11-2	C12-2	C22-2	116.2 (2)
N4-1	C13-1	C14-1	126.6 (2)	N4-2	C13-2	C14-2	125.8 (2)
N4-1	C13-1	C18-1	114.3 (2)	N4-2	C13-2	C18-2	114.7 (2)
C14-1	C13-1	C18-1	118.8 (2)	C14-2	C13-2	C18-2	119.0 (2)
C13-1	C14-1	C15-1	120.7 (2)	C13-2	C14-2	C15-2	120.2 (2)
C14-1	C15-1	C16-1	120.1 (2)	C14-2	C15-2	C16-2	120.8 (2)
C15-1	C16-1	C16-1	120.1 (2)	C15-2	C16-2	C16-2	119.9 (3)
C16-1	C17-1	C18-1	120.8 (2)	C16-2	C17-2	C18-2	120.5 (3)
N1-1	C18-1	C13-1	114.8 (2)	N1-2	C18-2	C13-2	114.4 (2)
N1-1	C18-1	C17-1	125.5 (2)	N1-2	C18-2	C17-2	125.8 (2)
C13-1	C18-1	C17-1	119.3 (2)	C13-2	C18-2	C17-2	119.5 (2)
Fe-1	O	Fe-2	142.75 (9)				
C2-A	C1-A	C2-A′	75.8 (4)				
C1-A	C2-A	N1-A	178.5 (8)				
C1-A	C2-A′	N1-A′	176.4 (8)				

Table VII. Angles (deg) between Selected Planes for $[Fe(C_{22}H_{22}N_4)]_2O\cdot CH_3CN$

defining planes between N1-1, N2-1, N3-1, N4-1 and	angle	defining planes between N1-2, N2-2, N3-2, N4-2 and	angle
N1-1, C1-1, C2-1, C3-1, N2-1	36.28	N1-2, C1-2, C2-2, C3-2, N2-2	36.03
N1-1, C1-1, C3-1, N2-1	36.69	N1-2, C1-2, C3-2, N2-2	36.32
N3-1, C10-1, C11-1, C12-1, N4-1	34.37	N3-2, C10-1, C11-2, C12-2, N4-2	35.98
N3-1, C10-1, C12-1, N4-1	34.99	N3-2, C10-2, C12-2, N4-2	36.86
N2-1, C4-1, C9-1, N3-1	13.63	N2-2, C4-2, C9-2, N3-2	14.14
N1-1, C18-1, C13-1, N4-1	14.41	N1-2, C18-2, C13-2, N4-2	14.32
C13-1, C14-1, C15-1, C16-1, C17-1, C18-1	19.57	C13-2, C14-2, C15-2, C16-2, C17-2, C18-2	18.69
C4-1, C5-1, C6-1, C7-1, C8-1, C9-1	19.28	C4-2, C5-2, C6-2, C7-2, C8-2, C9-2	20.19

In the two structures $[Fe(C_{22}H_{22}N_4)]_2O$ and $[Fe(C_{22}H_{22}N_4)Cl]$ the Fe–O and Fe–Cl bond distances are systematically longer than in their tetraphenylporphyrin counterparts. The longer axial bond distances are a consequence of two factors: the charge delocalization in the inner ring is limited to the 2,4-pentanediiminato chelate rings and the Fe–N distances are considerably shorter than in the TPP^{2-} complexes. Thus the charge donation to the central metal ion is larger

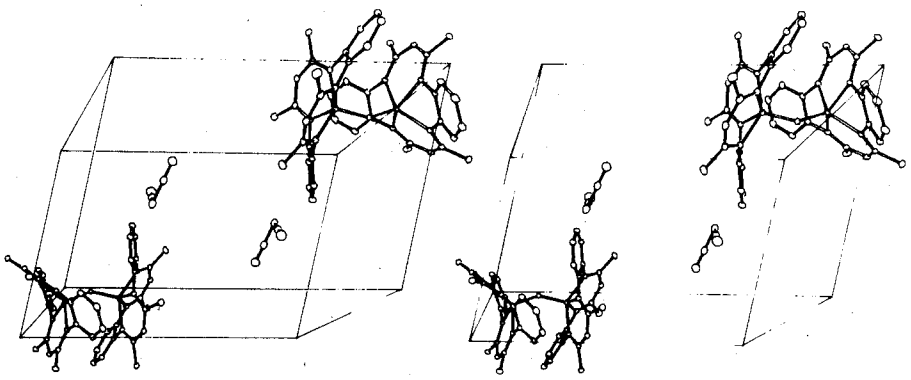

Figure 4. Stereoscopic diagram of the unit cell contents and packing arrangement of $[Fe(C_{22}H_{22}N_4)]_2O{\cdot}CH_3CN$ as viewed down the axis normal to the *ac* crystallographic face. The acetonitrile molecule is shown in its disordered configuration. The thermal ellipsoids are drawn at the 10% probability level.

Table VIII. Selected Dihedral Angles (deg) for $[Fe(C_{22}H_{22}N_4)]_2O{\cdot}CH_3CN$

atoms defining planes			angle	atoms defining planes			angle
C19-1	C1-1	N1-1		C19-2	C1-2	N1-2	
C1-1	N1-1	C18-1	1.8 (3)	C1-2	N1-2	C18-2	2.7 (2)
C20-1	C3-1	N2-1		C20-2	C3-2	N2-2	
C3-1	N2-1	C4-1	4.1 (3)	C3-2	N2-2	C4-2	2.9 (3)
C21-1	C10-1	N3-1		C21-2	C10-2	N3-2	
C10-1	N3-1	C9-1	2.2 (3)	C10-2	N3-2	C9-2	1.0 (3)
C22-1	C12-1	N4-1		C22-2	C12-2	N4-1	
C12-1	N4-1	C13-1	0.7 (3)	C12-2	N4-2	C13-1	1.5 (3)
C1-1	N1-1	C18-1		C1-2	N1-2	C18-2	
N1-1	C18-1	C17-1	49.0 (3)	N1-2	C18-2	C17-2	50.1 (3)
C3-1	N2-1	C4-1		C3-2	N2-2	C4-2	
N2-1	C4-1	C5-1	49.1 (3)	N2-2	C4-2	C5-2	46.3 (3)
C10-1	N3-1	C9-1		C10-2	N3-2	C9-2	
N3-1	C9-1	C8-1	50.5 (3)	N3-2	C9-2	C8-2	46.0 (3)
C12-1	N4-1	C13-1		C12-2	N4-2	C13-2	
N4-1	C13-1	C14-1	40.8 (3)	N4-2	C13-2	C14-2	50.0 (3)

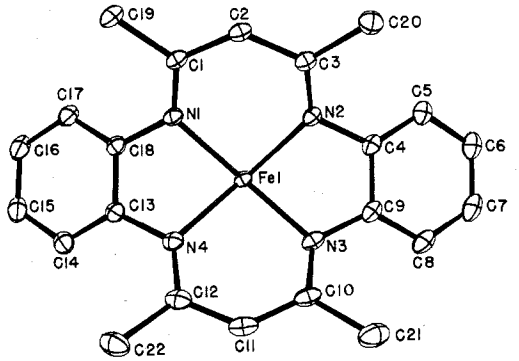

Figure 5. Projection down the Fe–O bond axis of half of the dimer $[Fe(C_{22}H_{22}N_4)]_2O$ illustrating the labeling scheme referred to in the tables of bond distances and angles.

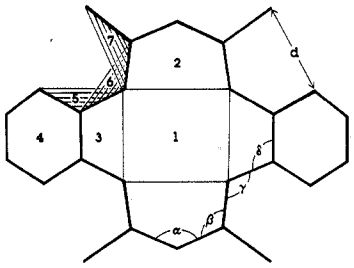

Figure 6. Diagrammatic representation of the $C_{22}H_{22}N_4^{2-}$ framework with "key" notations to assist the tabulation of important average parameters.

than that from the fully delocalized porphyrin ligand. The longer axial bond distances in the $C_{22}H_{22}N_4^{2-}$ complexes are thus the result of decreased electrostatic component to the Fe–axial bonds.

Both macrocyclic ligands ($C_{22}H_{22}N_4^{2-}$ and TPP) have some flexibility with regard to the N–Ct distance. However, the larger N–Ct distances associated with the 16-membered inner ring of the porphyrin skeleton reduces the need for the Fe(III) atoms to be elevated as much from the N_4 plane to allow reasonable Fe–N bond distances. Since the N–Ct distances in the Fe(III) species with the $C_{22}H_{22}N_4^{2-}$ ligand are smaller than in their porphyrin counterparts, an increased Fe–N_4 distance is required to accommodate the idealized Fe–N distances. This is accomplished, as mentioned earlier, by the increase in the angles associated with the inner ring (Figure 6) and the large torsional twists about the C–N bonds of the five-membered chelate ring.

Table IX. Structural and Magnetic Parameters for Some μ-Oxo-Fe(III) Dimers

compd	Fe–O,[a] Å	Fe–N-(O),[b] Å	Fe–N_4-(N_2O_2),[c] Å	N–Ct,[d] Å	Fe–O–Fe, deg	μ_{eff}, μ_B	ref
$[Fe(C_{22}H_{22}N_4)]_2O{\cdot}CH_3CN$[e]	1.792	2.054	0.698	1.931	142.75	1.96	this work
$[Fe(TPP)]_2O$[f]	1.763	2.087	0.50	2.027	174.5	1.8–1.9	2, 3, 18, 19
$[Fe(HEDTA)]_2O^{2-}$[g]	1.79	2.25 2.03	0.36		165.0		4
$[Fe(salen)]_2O{\cdot}CH_2Cl_2$[h]	1.794	2.105 1.922	0.56		142.2	1.99	5, 20
$[Fe(salen)]_2O{\cdot}2py$[h]	1.80	2.09 1.93	0.56		139.0	1.90	6, 7
$[FeB(H_2O)]_2O$[i]	1.8	2.2	*j*	*j*	*j*		11

[a] Fe to bridging O^{2-} ligand distance. [b] Fe to N or O equatorial ligand distance; when only one value is listed it corresponds to a N donor; when two values are listed they correspond to N and O donors, respectively. [c] Distance of Fe atom from the equatorial plane defined by N_4 or N_2O_2 donor atoms. [d] Ideal N to center of macrocycle core distance. [e] $C_{22}H_{22}N_4^{2-} = L^{2-}$. [f] $TPP^{2-} \equiv$ mesotetraphenylporphyrin. [g] $HEDTA^- \equiv$ *N*-hydroxyethylethylenediaminetriacetato(1–). [h] salen ≡ *N*,*N*′-ethylenebis(salicylideniminato)(1–). [i] B ≡ 2,13-dimethyl-3,6,9,12,18-pentaazabicyclo[12.3.1]octadeca-1(18),2,12,14,16-pentaene. [j] Not given.

Table X. Summary of Important Parameters for $[Fe(C_{22}H_{22}N_4)]_2O\cdot CH_3CN$ and $[Fe(C_{22}H_{22}N_4)Cl]\cdot CH_3CN$ with Comparisons with Analogous Mesotetraphenylporphyrin Complexes

	$[Fe(C_{22}H_{22}N_4)]_2O\cdot CH_3CN$	$[Fe(C_{22}H_{22}N_4)Cl]\cdot CH_3CN$[a]
av Fe–N dist, Å	2.054 (2.087)[b]	2.002 (2.049)[c]
av Fe–N_4 dist,[c] Å	0.698 (0.500)[b]	0.600 (0.380)[c]
av Ct–N dist, Å	1.931 (2.027)[b]	1.910 (2.012)[c]
av Fe–axial ligand dist, Å	1.792 (1.763)[b]	2.252 (2.192)[c]
av C–N dist (six-membered ring), Å	1.334	1.331
Av C–C dist (six-membered ring), Å	1.401	1.404
av C–N dist (five-membered ring), Å	1.412	1.422
av dihedral angles,[d,e] deg		
1–2	35.66	32.86
1–3	14.12	16.28
1–4	19.43	21.80
5–6	47.8	43.5
6–7	2.1	3.2
av bond angles,[d,e] deg		
α	129.5	129.6
β	122.3	121.5
γ	124.9	125.0
δ	114.5	113.9
av nonbonded dist, d,[c] Å	3.071	3.054
Fe–O–Fe angle, deg	142.75 (174.5)[b]	

[a] Values obtained from ref 12. [b] Number in parentheses refers to corresponding distance in $[Fe(TPP)]_2O$.[2,3] [c] Number in parentheses refers to corresponding distance in [Fe(TPP)Cl].[40] [d] Fe–N_4 refers to the distance of Fe from the N_4 donor plane. [e] See Figure 6 for key.

The parallels exhibited by these two pairs of structures indicate that other analogues of the iron porphyrin complexes may have the same coordination behavior. Indeed, this has been demonstrated in the carbon monoxide structures of [Fe(TPP)][43] and $[Fe(C_{22}H_{22}N_4)]$.[38] In light of the unusual reactivity associated with the tetramethyldibenzotetraaza-[14]annulene ligand, the reactivity and physical properties of the iron porphyrins in biologic systems may be mimicked.

Acknowledgment. M.C.W. is the recipient of a Medical Scientist National Research Service Award from the N.I.G.M.S., Grant No. 5T32GM07281. This research was supported in part by the National Institutes of Health, Grant No. HL 14827.

Registry No. $[Fe(C_{22}H_{22}N_4)]_2O\cdot CH_3CN$, 68423-91-6; $[Fe(o\text{-}PDA)_2(NCS)_2]$, 56370-61-7.

Supplementary Material Available: A listing of the observed and calculated structure factor amplitudes and hydrogen atom parameters (50 pages). Ordering information is given on any current masthead page.

References and Notes

(1) To whom correspondence should be addressed at the Department of Chemistry, The Florida State University, Tallahassee, Fla. 32306.
(2) E. B. Fleischer and T. S. Srivastava, *J. Am. Chem. Soc.*, **91**, 2403 (1969).
(3) A. B. Hoffman, D. M. Collins, V. W. Day, E. B. Gleischer, T. S. Srivastava, and J. L. Hoard, *J. Am. Chem. Soc.*, **94**, 3620 (1972).
(4) S. J. Lippard, H. Schugar, and C. Walling, *Inorg. Chem.*, **6**, 1825 (1967).
(5) P. Coggen, A. T. McPhail, F. E. Mabbs, and V. N. McLachlan, *J. Chem. Soc. A*, 1014 (1971).
(6) M. Gerloch, E. D. McKenzie, and A. D. C. Towl, *J. Chem. Soc. A*, 2850 (1969).
(7) M. Gerloch, E. D. McKenzie, and A. Towl, *Nature (London)*, **220**, 906 (1968).
(8) J. E. Davies and B. M. Gatehouse, *Acta Crystallogr., Sect. B*, **29**, 1934 (1973).
(9) J. E. Davies and B. M. Gatehouse, *Acta Crystallogr., Sect. B*, **29**, 2651 (1973).
(10) J. E. Davies and B. M. Gatehouse, *Acta Crystallogr., Sect. B*, **28**, 3641 (1972).
(11) E. B. Fleischer and J. Hawkinson, *J. Am. Chem. Soc.*, **89**, 721 (1967).
(12) M. C. Weiss, B. Bursten, S.-M. Peng, and V. L. Goedken, *J. Am. Chem. Soc.*, **98**, 8021 (1976).
(13) J. L. Hoard, G. H. Cohen, and M. D. Glick, *J. Am. Chem. Soc.*, **89**, 1922 (1967).
(14) J. L. Hoard, M. J. Hamor, T. A. Hamor, and W. S. Caughey, *J. Am. Chem. Soc.*, **87**, 2312 (1965).
(15) M. Gerloch and F. E. Mabbs, *J. Chem. Soc., A*, 1598 (1967).
(16) J. L. Hoard in "Porphyrins and Metalloporphyrins", K. M. Smith, Ed., Elsevier, Amsterdam, 1975.
(17) K. S. Murray, *Coord. Chem. Rev.*, **12**, 1 (1974).
(18) E. B. Fleischer, J. M. Palmer, T. S. Srivastava, and A. Chatterjee, *J. Am. Chem. Soc.*, **93**, 3162 (1971).
(19) I. A. Cohen, *J. Am. Chem. Soc.*, **91**, 1980 (1969).
(20) J. Lewis, F. E. Mabbs, and A. R. Richards, *J. Chem. Soc. A*, 1014 (1967).
(21) M. Gerloch, J. Lewis, F. E. Mabbs, and A. Richards, *J. Chem. Soc. A*, 112 (1968).
(22) G. N. LaMar, G. R. Eaton, R. H. Holm, and F. A. Walker, *J. Am. Chem. Soc.*, **95**, 63 1973).
(23) P. D. W. Boyd and T. D. Smith, *Inorg. Chem.*, **10**, 2041 (1971).
(24) W. S. Caughey, *Adv. Chem. Ser.*, **No. 100**, 248 (1971).
(25) R. H. Felton, G. S. Owen, D. Dolphin, and J. Fajer, *J. Am. Chem. Soc.*, **93**, 6332 (1971).
(26) M. Wicholas, R. Mustacich, and D. Jayne, *J. Am. Chem. Soc.*, **94**, 4518 (1972).
(27) P. D. W. Boyd and K. S. Murray, *J. Chem. Soc. A*, 2711 (1971).
(28) For related chemistry and structures see: M. C. Weiss, B. Bursten, S.-M. Peng, and V. L. Goedken, *J. Am. Chem. Soc.*, **98**, 8500 (1976); M. C. Weiss and V. L. Goedken, *ibid.*, **98**, 3389 (1976); V. L. Goedken, S.-M. Peng, J. Molin-Norris, and Y.-A. Park, *ibid.*, **98**, 8391 (1976).
(29) (a) V. L. Goedken, J. Molin-Case, and Y.-A. Park, *J. Chem. Soc., Chem. Commun.*, 337 (1973); (b) D. R. Neves and J. C. Dabrowiak, *Inorg. Chem.*, **15**, 129 (1976).
(30) "International Tables for X-ray Crystallography", Vol. 1, 2nd ed., Kynoch Press, Birmingham, England, 1965.
(31) L. V. Azaroff, *Acta Crystallogr.*, **8**, 701 (1955).
(32) W. Busing and H. H. Levy, *J. Chem. Phys.*, **26**, 563 (1957).
(33) P. W. R. Corfield, R. Doedens, and J. A. Ibers, *Inorg. Chem.*, **68** 197 (1967).
(34) Computations were performed by IBM computer with the aid of the following programs: Zalkin's FORDAP Fourier program, Busing and Levy's ORFFE function and error program, and Ibers' NUCLS least-squares program. Plots of the structures were drawn with the aid of C. K. Johnson's ORTEP.
(35) Neutral atom scattering factors were taken from D. T. Cromer and J. B. Mann, *Acta Crystallogr., Sect. A*, **24**, 321 (1968). Hydrogen atom scattering factors were taken from "International Tables for X-ray Crystallography", Vol. III, Kynoch Press, Birmingham, England, 1962. Anomalous scattering corrections were applied to heavy atoms and were taken from D. T. Cromer, *Acta Crystallogr.*, **18**, 17 (1965).
(36) M. R. Churchill, *Inorg. Chem.*, **12**, 1213 (1973).
(37) Supplementary material.
(38) V. L. Goedken, S.-M. Peng, J. Molin-Norris, and Y.-A. Park, *J. Am. Chem. Soc.*, **98**, 8391 (1976).
(39) V. L. Goedken, J. J. Pluth, S.-M. Peng, and B. Bursten, *J. Am. Chem. Soc.*, **98**, 8014 (1976).
(40) J. L. Hoard, G. H. Cohen, and M. D. Glick, *J. Am. Chem. Soc.*, **89**, 1922 (1967); D. F. Koenig, *Acta Crystallogr.*, **18**, 663 (1965).
(41) K. N. Raymond, D. W. Meek, and J. A. Ibers, *Inorg. Chem.*, **7**, 1111 (1968).
(42) M. Yevitz and J. A. Stanko, *J. Am. Chem. Soc.*, **93**, 1512 (1971).
(43) S.-M. Peng and J. A. Ibers, *J. Am. Chem. Soc.*, **98**, 8032 (1976).
(44) V. L. Goedken, S.-M. Peng, and Y.-A. Park, *J. Am. Chem. Soc.*, **96**, 284 (1974).